ELSEVIER

Journal of Alloys and Compounds 297 (2000) 294–302

Journal of ALLOYS AND COMPOUNDS

www.elsevier.com/locate/jallcom

Martensitic transformation of a Ti-rich $Ti_{40.5}Ni_{49.5}Zr_{10}$ shape memory alloy

S.K. Wu[a,*], S.F. Hsieh[b]

[a]*Institute of Materials Science and Engineering, National Taiwan University, Taipei, Taiwan 106, ROC*
[b]*Dept. of Mold and Die Engineering, National Institute of Science and Technology, Kaohsiung, Taiwan 807, ROC*

Received 6 February 1999; accepted 13 September 1999

Abstract

$Ti_{40.5}Ni_{49.5}Zr_{10}$ alloy undergoes a B2↔B19′ one-stage martensitic transformation with Ms≈100°C. This alloy exhibits about 90% shape memory recovery even though many $(Ti,Zr)_2Ni$ particles exist around (Ti,Zr)Ni grain boundaries. The B19′ martensite structure is calculated with $a=0.295$ nm, $b=0.408$ nm, $c=0.491$ nm and $\beta=97.4^0$. Martensitic transformation temperatures decrease with increasing aging time at 300°C. This feature is a result of the aging effect of point defects/atoms rearrangement in B2 phase. Thermal cycling can also decrease transformation temperatures while increasing the hardness of the alloy. The strengthening effects of aging and thermal cycling on the Ms (M*) temperature of $Ti_{40.5}Ni_{49.5}Zr_{10}$ alloy can be represented by the equation $Ms=T_o-K\,\Delta\sigma_y$. Experimental results indicate that martensitic transformation temperatures of $Ti_{40.5}Ni_{49.5}Zr_{10}$ alloy can be more effectively depressed by aging than by thermal cycling.

Keywords: Martensitic transformation; Shape memory; Titanium alloy

1. Introduction

TiNi alloys are known as the most important shape memory alloys (SMAs) due to their excellent shape-memory effect and pesudoelasticity. However, they are limited to use at temperatures lower than 150°C because their martensitic transformation starting temperature, Ms, is usually lower than 100°C. High-temperature SMAs with an Ms temperature higher than 100°C have been extensively researched due to their potential applications. It is well known that $Ti_{50}Ni_{50-Y}X_Y$ ternary SMAs with X=Pd, Pt or Au have an Ms temperature much higher than 100°C and exhibit an one-way shape memory effect [1–3]. However, the high cost of precious metals will limit the practical applications of these SMAs. For this reason, other ternary TiNiX SMAs of lower costs need to be investigated. Among them, the most prospective candidates are TiNiZr and TiNiHf alloys with Zr and Hf replacing Ti in these alloys.

Three phases, (Ti,Zr)Ni, $(Ti,Zr)_2Ni$ and the λ_1 phase are observed in Ti-rich $Ti_{53-X}Ni_{47}Zr_X$ alloys with the Zr content in the range of 5~20 at.% at room temperature [4]. Here, λ_1 phase is a TiNiZr ternary solid solution and the (Ti,Zr)Ni phase can exhibit the B2↔B19′ martensitic transformation with the Ms temperature in the range of 60°C ~260°C [4]. Hsieh et al. [5] reported that the lattice parameters of martensitic phase B19′ by using the XRD, TEM and Riverted method [6] are dependent on the Zr content in $Ti_{50.5-X}Ni_{49.5}Zr_X$ SMAs with Zr content in the range of 1–20 at.% at room temperature. Meanwhile, Mulder et al. [7] reported that the Ms temperatures above 120°C can be obtained in TiNiZr alloys with Zr content above 10 at.% and Ni content below 49.5 at.%. They also found that the decrease in transformation temperatures in the thermal-cycled $Ti_{31.5}Ni_{48.5}Zr_{20}$ alloy is affected by the $(Ti,Zr)_2Ni$ precipitates.

It has been confirmed that the transformation characteristics of Ti-rich binary TiNi SMAs can be affected by various thermo-mechanical treatments, such as thermal cycling, aging and cold rolling [8]. However, few reports have been made on Ti-rich TiNiZr ternary alloys [9] whose transformation behaviors and shape-memory characteristics are affected by different thermo-mechanical treatments. In

*Corresponding author.
E-mail address: skw@ccms.ntu.edu.tw (S.K. Wu)

0925-8388/00/$ – see front matter
PII: S0925-8388(99)00604-0

the present study, we aim to understand the general characteristics of a Ti-rich $Ti_{40.5}Ni_{49.5}Zr_{10}$ ternary alloy, including transformation temperatures, microstructures and internal friction properties, etc. The variation of martensitic transformation temperatures with aging time and the effect of thermal cycling on this alloy will also be discussed.

2. Experimental procedure

The conventional tungsten arc melting technique was employed to prepare the $Ti_{40.5}Ni_{49.5}Zr_{10}$ (at.%) alloy. Titanium (purity 99.7%), nickel (purity 99.9%) and aluminum (purity 99.9%), totaling about 120 g, were melted and remelted at least six times in an argon atmosphere. A pure titanium button was used as a getter during the arc melting. Weight loss during melting was negligibly small. The as-melted ingots were homogenized at 950°C×72 h and then quenched in water. They were swaged at 800°C×1 h and then annealed at 850°C×1 h. Specimens were cut into several plates with a low speed diamond saw, and then annealed at 900°C×1 h and finally quenched in water. After the annealing treatment, two experimental procedures were conducted. First, several plates were sealed in evacuated quartz tubes and aged at 300°C for 1–240 h and then quenched in water. Second, several more plates were subjected to thermal cycling N times from 0°C to 300°C with N=1~100 cycles. Specimens for electrical resistivity measurement (size: 50 mm× 1 mm×1 mm), DSC measurement, internal friction test (size: 110 mm×4 mm×1 mm), hardness test, shape recovery test and microstructure observation were carefully cut from plates treated using the above procedures.

Martensitic transformation temperatures were measured by using a four-probe electrical resistivity. The temperature range for electrical resistivity test was from 25°C to +250°C. DSC measurements were made with a Dupont 9990 thermal analyzer equipped with a quantitative scanning system 910 DSC cell for controlled heating and cooling runs on samples encapsulated in an aluminum pan. The running temperature range was from 0°C to +200°C with a heating and cooling rate of 10°C/min. An internal friction (IF) test was carried out with a SINKU-RIKO 1500 M/L series inverted torsion pendulum in the temperature range from −150°C to +250°C. The temperature rate was precisely controlled at 2°C/min and the test frequency was approximately 1 Hz. Specimens for the hardness test were first mechanically polished and then subjected to measurement in a microvickers hardness tester with 500 g load at room temperature. For each specimen, the average hardness value was taken from at least five test readings. The microstructure observations were made using optical microscope (OM) and transmission electron microscope (TEM). The shape recovery measurement was performed as described earlier by Lin et al. [10]. A quantitative analysis of the chemical composition of the phases was performed by using a JOEL JXA-8600SX electron probe microanalyzer (EPMA) equipped with a WDX analysis system. TEM specimens were prepared by electropolishing at 0°C with an electrolyte consisting of 20% H_2SO_4 and 80% CH_3OH by volume. Selected area diffraction patterns (SADPs) and TEM images were examined using a JEOL-4000FX microscope equipped with an energy dispersive X-ray (EDX) system.

3. Results and discussion

3.1. Transformation behavior in $Ti_{40.5}Ni_{49.5}Zr_{10}$ alloy

Fig. 1 shows the experimental results of electrical resistivity versus temperature for the annealed $Ti_{40.5}Ni_{49.5}Zr_{10}$ alloy. The notation for the determination of martensitic transformation temperatures, Ms, M_f, As and A_f, in Fig. 1 follows the example established by Hwang et al. [11]. The martensitic transformation starts at Ms (≈100°C), where the resistance is at a minimum but increases quickly until M_f (≈75°C) is reached. Upon heating from 25°C, the resistance increases up to As (≈135°C), where the slope of the curve changes and continuously decreases down to A_f (≈175°C). This stage corresponds to the reverse transformation from martensite to B2 parent phase.

Fig. 2a shows the TEM bright field image of martensite in annealed $Ti_{40.5}Ni_{49.5}Zr_{10}$ alloy. Figs. 2b–d are SADPs of Fig. 2a, in which the foil is tilted to parallel the $[100]_M$, $[0\bar{1}1]_M$ and $[\bar{1}11]_M$ direction, respectively. Han et al. found that lattice parameters of martensite in $Ti_{36.5}Ni_{48.5}Hf_{15}$ alloy is a monoclinic structure with a=0.293 nm, b=0.411 nm, c=0.473 nm and β=100.4° [12]. The SADPs of this annealed alloy coincide with those of Han's results. Therefore, based on Fig. 2 and Ref. [5], we can calculate the martensite structure of $Ti_{40.5}Ni_{49.5}Zr_{10}$ alloy and find

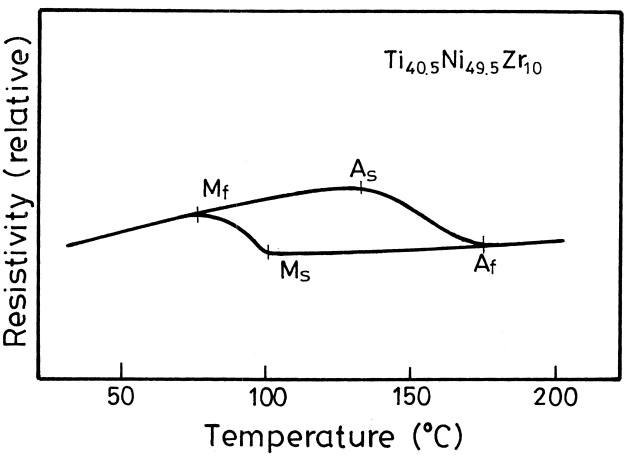

Fig. 1. Electrical resistivity versus temperature curve for 900°C×1 h annealed and water quenched $Ti_{40.5}Ni_{49.5}Zr_{10}$ alloy.

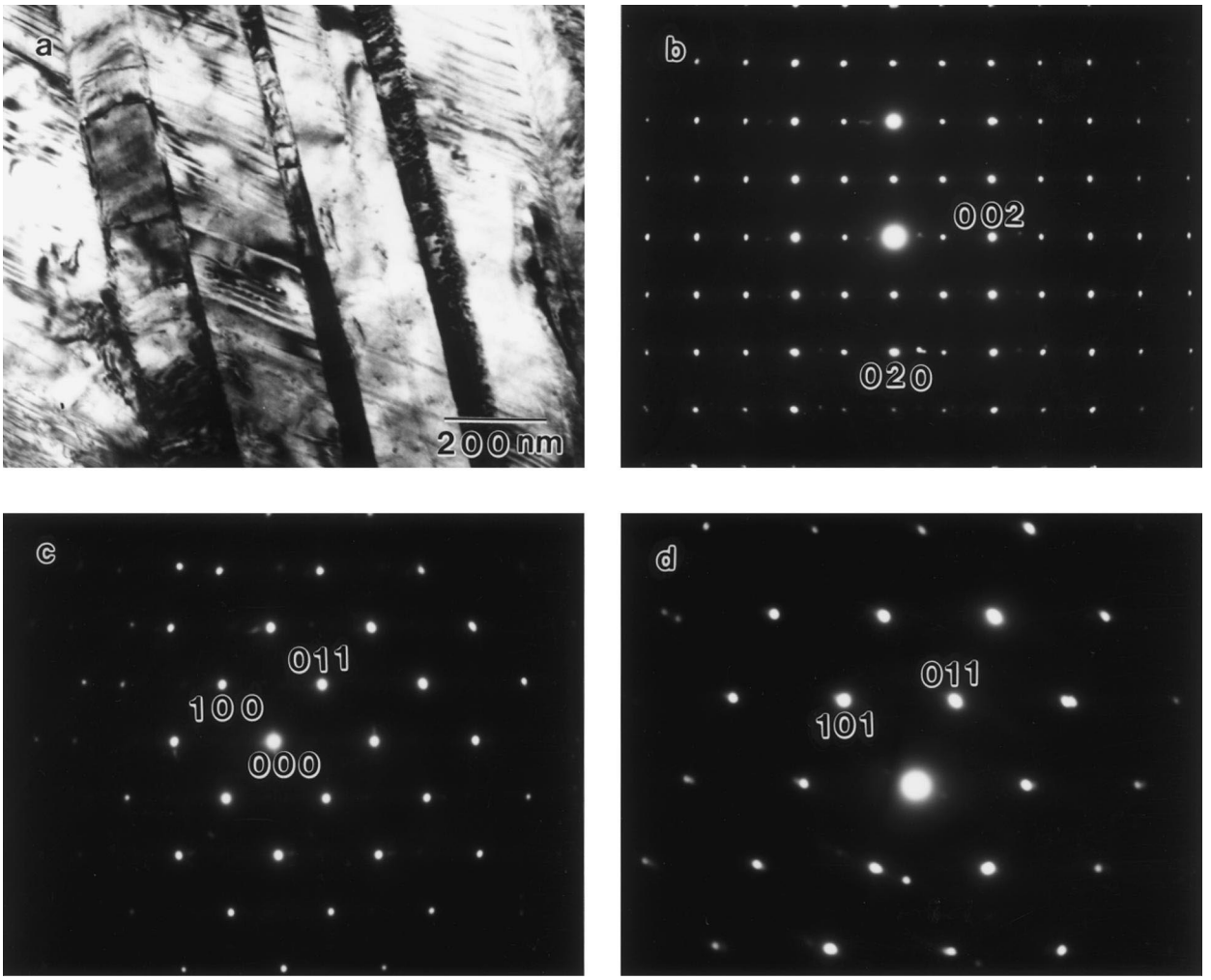

Fig. 2. (a) TEM bright-field image of as-annealed $Ti_{40.5}Ni_{49.5}Zr_{10}$ alloy. (b) SADP of (a) with $[100]_M$ zone axis, (c) SADP of (a) with $[01\bar{1}]_M$ zone axis, (d) SADP of (a) with $[11\bar{1}]_M$.

that it is also a monoclinic B19′ structure in which $a=0.295$ nm, $b=0.408$ nm, $c=0.481$ nm and $\beta=97.4°$.

Fig. 3 shows the OM microstructure of $Ti_{40.5}Ni_{49.5}Zr_{10}$ alloy. A great number of second phase particles are found around B2 grain boundaries. The chemical compositions of matrix and second-phase particles found using EPMA analysis are (Ti,Zr)Ni and $(Ti,Zr)_2Ni$, respectively, as shown in Table 1. In spite of the existence of many particles, this alloy still exhibits rather good shape recovery, which can reach about 90%, as shown in Fig. 4.

Fig. 5a and b show the IF test result and plot the frequency f (shear modulus) and Q^{-1}_{max} versus temperature of the annealed $Ti_{40.5}Ni_{49.5}Zr_{10}$ alloy. In Fig. 5b, there is one peak P_C at 84°C on cooling and one peak P_H at 151°C on heating. Both peaks, which correspond to the minimum of frequency f shown in Fig. 5a, indicate the minima of the shear modulus. The peak P_R appearing at −38°C which does not correspond to the minimum of frequency f is proposed to be a relaxation peak. The relaxation peak is suggested to be associated with the interaction of disloca-

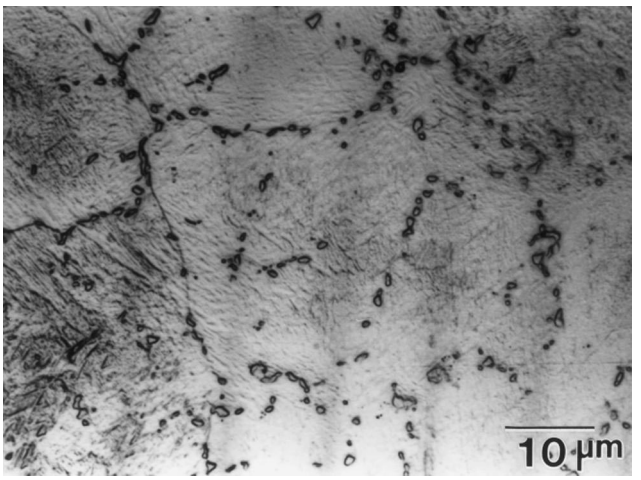

Fig. 3. Optical micrographic microstructure of as-annealed $Ti_{40.5}Ni_{49.5}Zr_{10}$ alloy.

Table 1
EPMA analysis for $Ti_{40.5}Ni_{49.5}Zr_{10}$ alloy annealed at 950°C×72 h

$Ti_{40.5}Ni_{49.5}Zr_{10}$ alloy	Composition (at.%)		
	Ti	Ni	Zr
Matrix	40.81	49.01	10.18
Second phase	56.52	33.19	10.29

tions and point defects [13], and is independent of the martensite and premartensite transformations [14]. The temperature difference ΔT between P_H and P_C is approximately 67°C for this alloy, which is larger than that of $Ti_{51}Ni_{49}$ alloy (ΔT=41°C) [8]. This feature indicates that the Zr atoms solid-soluted in Ti-rich TiNi alloy will result in a different chemical free energy between binary TiNi and ternary TiNiZr SMAs. The height Q^{-1}_{max} (3.12×10^{-2}) of internal friction peak, P_C, in Fig. 5 is lower than that of $Ti_{51}Ni_{49}$ alloy ($Q^{-1}_{max}=5.2\times10^{-2}$ with the same specimen size) [8]. This characteristic show that the solid solution hardening in Ti-rich TiNiZr alloys may decrease the mobility of twin plates in the martensite and that of the interfaces between martensite and parent phase. From Figs. 1, 2 and 5, one can find that the transformation sequence of martensite in $Ti_{40.5}Ni_{49.5}Zr_{10}$ alloy is the B2↔B19′ one-stage transformation.

3.2. Effects of aging and thermal cycling on Ti-rich $Ti_{40.5}Ni_{49.5}Zr_{10}$ alloy

Fig. 6a and b show the same plots as Fig. 5, but now for the alloy aged at 300°C×120 h. In Fig. 6b, there is one peak P_C on cooling, and one peak P_H on heating in the first cycle. Peaks P_C and P_H are associated with the martensitic transformation. A well-shaped relaxation peak P_R appears at −27°C, which does not correspond the minimum of frequency of f in Fig. 6a. The plots of different aging times of this alloy are similar to those of Fig. 6, except that the temperatures P_C, P_H and P_R and the magnitude of Q^{-1}_{max} are different, and are thus omitted here. Pc, P_H, P_R versus the aging time of this alloy derived from the internal friction test are plotted in Fig. 7. From Fig. 7, P_C, P_H and P_R are all affected by aging time. Fig. 8 shows that the Hv hardness of the 300°C aged $Ti_{40.5}Ni_{49.5}Zr_{10}$ alloy increases significantly in the first 40 h and then gradually levels off with further aging.

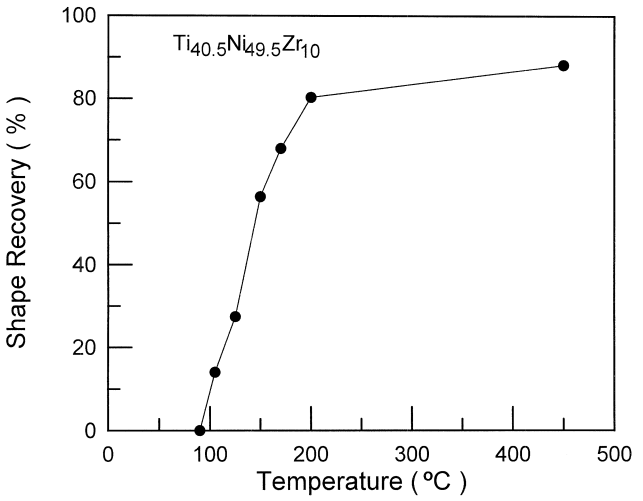

Fig. 4. Shape recovery versus heating temperature for $Ti_{40.5}Ni_{49.5}Zr_{10}$ alloy.

Fig. 9a shows a TEM bright-field image of the B19′ martensite in a 300°C ×240 h aged $Ti_{40.5}Ni_{49.5}Zr_{10}$ alloy. Fig. 9b shows the SADPs taken from the martensite plate having fine striations at area *E* of Fig. 9a, in which the foil is parallel to $[110]_M$ direction. No extra reflection spot can be observed in Fig. 9 except for the $(001)_M$ compound twins. Thus, the fine striations are traces of $(001)_M$ twins plates. The $(001)_M$ compound twins and $[011]_M$ type II twins are the substructures of the martensite in the aged $Ti_{36.5}Ni_{48.5}Hf_{15}$ alloy, which have many defects such as dislocations [15]. Similar microstructures can also be observed in Fig. 9. Compared with Figs. 9 and 2, $(001)_M$ twin planes of the aged specimen are more dense than those of the annealed one. This result may indicate that $(001)_M$ compound twins of the aged specimen have a lower stacking fault energy than those of the annealed one. From Fig. 7, transformation temperatures of P_C and P_H decrease with increasing aging time, most likely a result of the following aging effects: (i) The interstitial atoms (such as H, O, etc.) can be solid-soluted in specimens during the arc melting process and excess vacancies can be obtained by quenching the annealed specimen at 900°C. The aging process causes the interstitial atoms to rearrange and eliminate excess vacancies. Therefore, the interfaces between parent phase and martensite during the martensitic transformation may be impeded by these point defects in aged specimens. (ii) The Zr atoms replace Ti atoms in $Ti_{40.5}Ni_{49.5}Zr_{10}$ alloy due to the isomorphologic solid solution effects of Ti and Zr atoms in the Ti–Zr binary phase diagram [16]. The excess quenched-in-vacancies can promote atomic rearrangement of Ti and Zr atoms in the B2 parent phase during the aging process. This reordered process may introduce microstrain field/lattice distortion and result in the hardness increment, as shown in Fig. 8. The lattice distortion will hinder the mobility of twin plates in martensite and/or that of interfaces between the martensite and parent phase. The aged specimens have finer $(001)_M$ compound twins and more dislocations, as shown in Fig. 9, most likely a result of the above mentioned aging effects of (i) and (ii).

Table 2 shows the DSC forward peak temperature M* and the hardness Hv of the thermal-cycled $Ti_{40.5}Ni_{49.5}Zr_{10}$ alloy. From Table 2, the M* temperatures decrease, but the hardness Hv increases with increasing thermal cycling, resulting from the effect of dislocations induced by thermal cycling, as proposed in thermal-cycled binary TiNi SMAs [17].

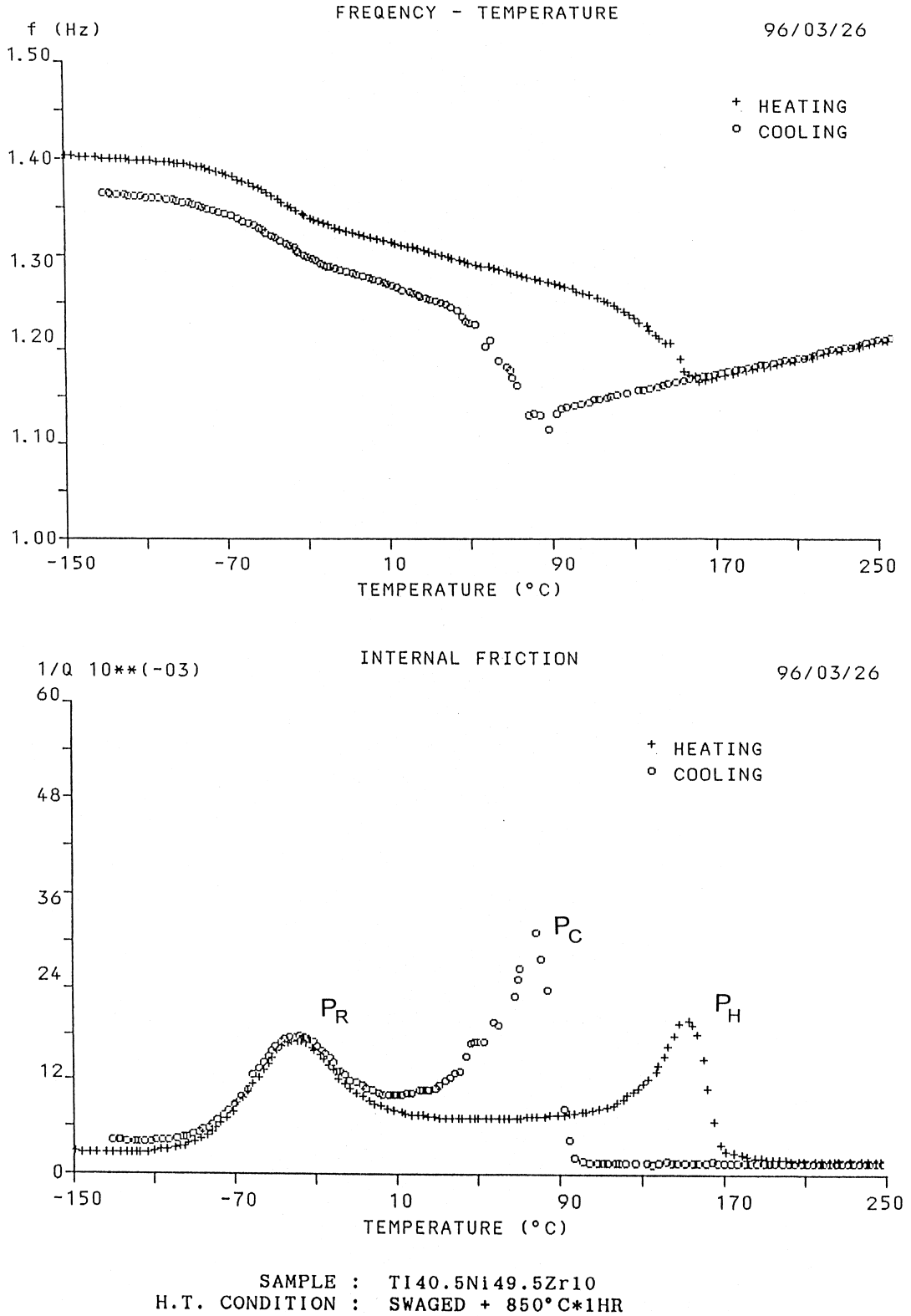

Fig. 5. (a) Frequency, f, and (b) internal friction, Q^{-1}_{max}, versus temperature for the annealed $Ti_{40.5}Ni_{49.5}Zr_{10}$ alloy. Peaks P_C and P_H are associated with the martensitic transformation and peak P_R is a relaxation one.

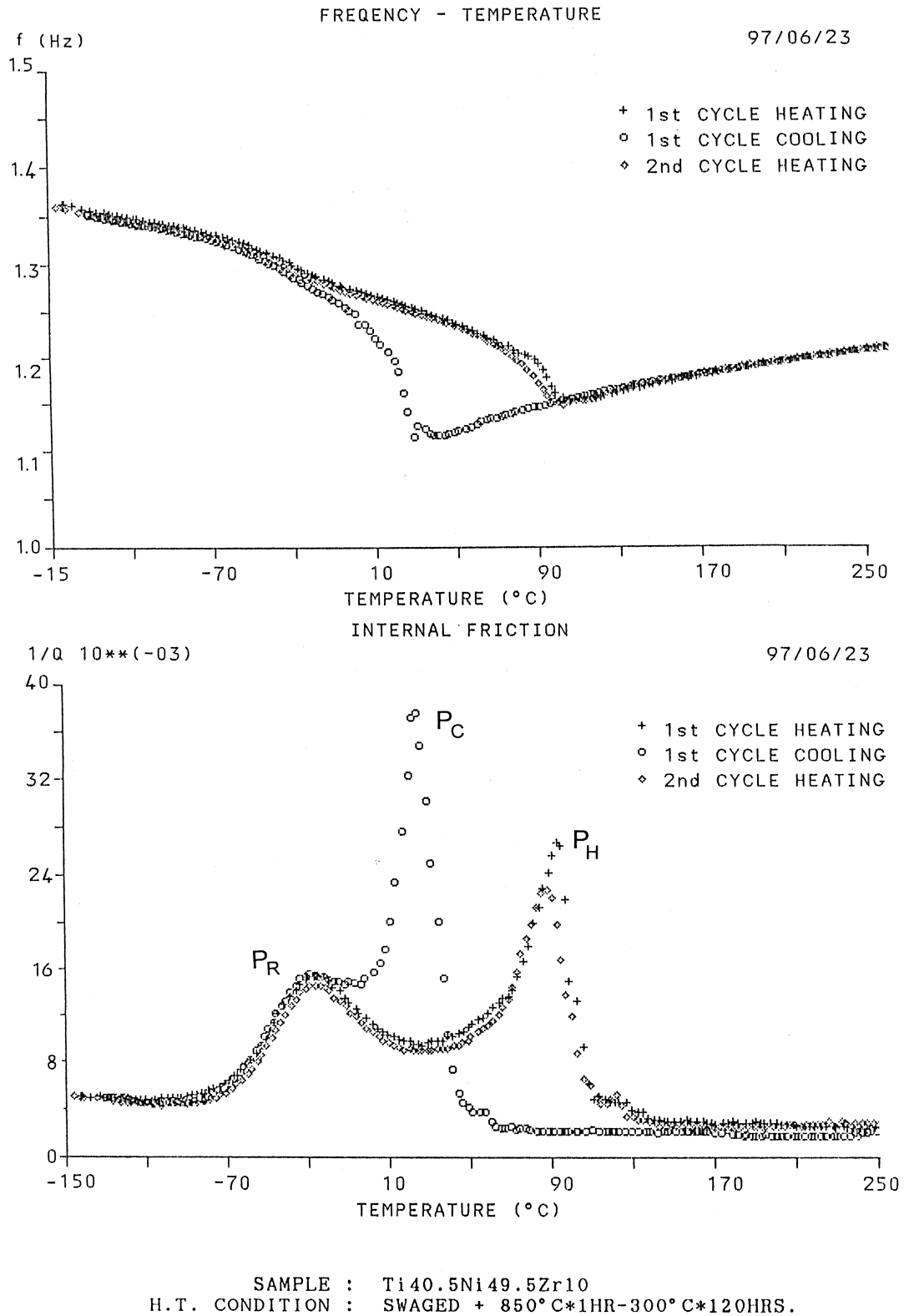

Fig. 6. (a) Frequency, *f*, and (b) internal friction, Q^{-1}_{max}, versus temperature of $Ti_{40.5}Ni_{49.5}Zr_{10}$ alloy aged at 300°C for 120 h. Peaks P_C and P_H are associated with the martensitic transformation and peak P_R is a relaxation one.

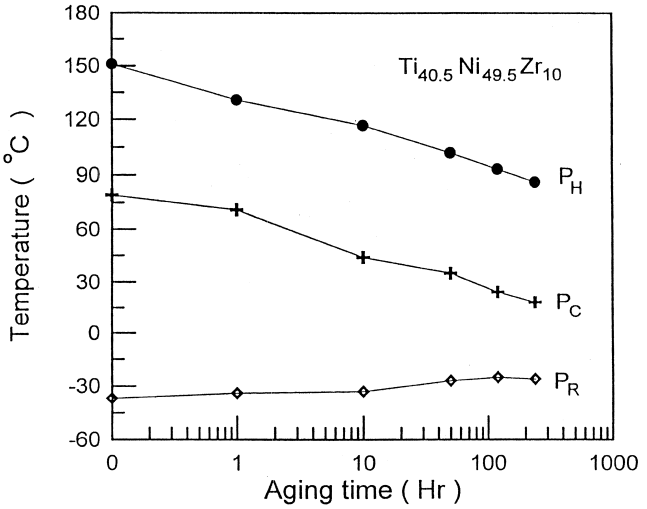

Fig. 7. The peak temperatures of P_H, P_C and P_R versus aging time for $Ti_{40.5}Ni_{49.5}Zr_{10}$ alloy aged at 300°C.

3.3. Strengthening effects in the aged and thermal-cycled Ti-rich $Ti_{40.5}Ni_{49.5}Zr_{10}$ alloy

Fig. 10 shows the curves of DSC peak temperature M* vs. hardness Hv for the thermal-cycled and aged $Ti_{40.5}Ni_{49.5}Zr_{10}$ alloy. The results of the thermal-cycled Ti-rich $Ti_{51}Ni_{49}$ alloy are also plotted in Fig. 10. It was pointed out that any strengthening mechanism which impedes the transformation shear can lower transformation temperatures because martensitic transformation involves a shear process [18,19]. This feature can be expressed by Eq. (1).

$$Ms = T_o - K\,\Delta\sigma_y \quad (1)$$

The constant K contains the factors of proportionality between the critical shear stress and the yield stress $\Delta\sigma_y$, the equilibrium temperature T_o is a function of the chemical composition, and the yield stress $\Delta\sigma_y$ is considered to be proportional to the hardness.

In this study, thermal cycling and aging processes do not change the alloy's composition, hence T_o is a constant. In addition, thermal cycling and aging can cause the alloy's

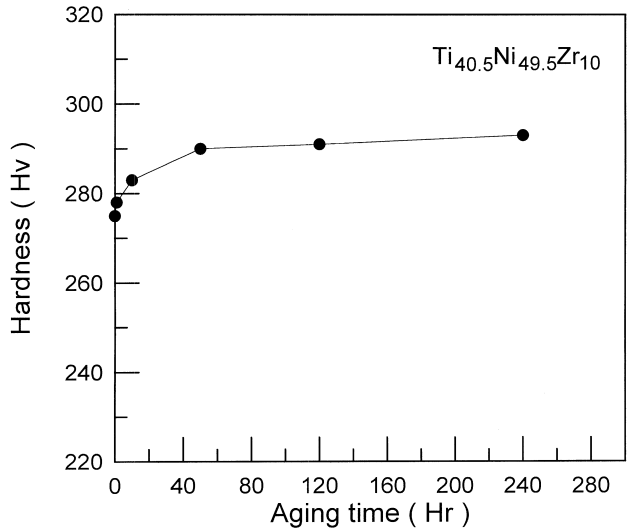

Fig. 8. Hardness versus aging time for 300°C aged $Ti_{40.5}Ni_{49.5}Zr_{10}$ alloy.

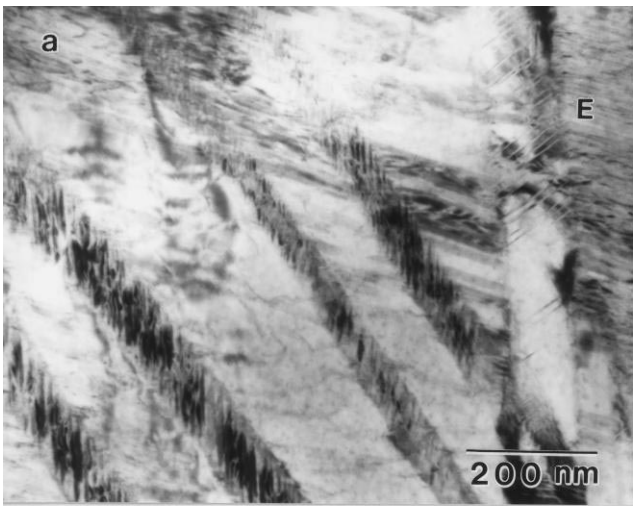

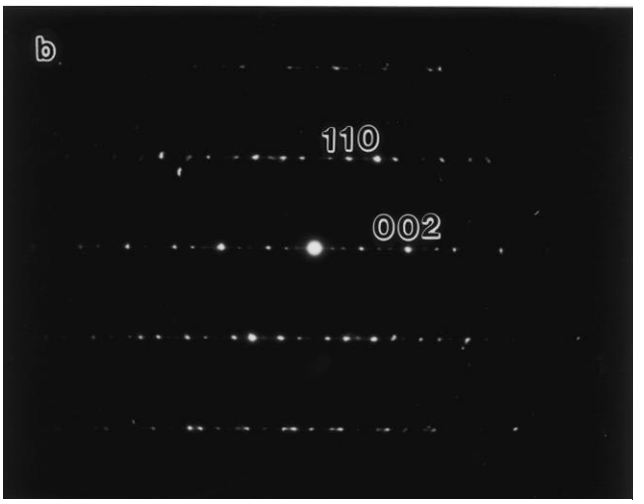

Fig. 9. (a) TEM bright-field image of $Ti_{40.5}Ni_{49.5}Zr_{10}$ alloy aged at 300°C for 240 h. (b) SADP taken from area E in (a), showing $(001)_M$ compound twins with $[110]_M$ zone axis.

Table 2
DSC forward peak temperatures M* and hardness Hv for various thermal cycled $Ti_{40.5}Ni_{49.5}Zr_{10}$ alloy

Thermal cycles (N)	$Ti_{40.5}Ni_{49.5}Zr_{10}$ alloy	
N	M*(°C)	Hardness (Hv)
1	84	273
2	78	286
10	66	300
20	58	310
50	54	322
100	50	330

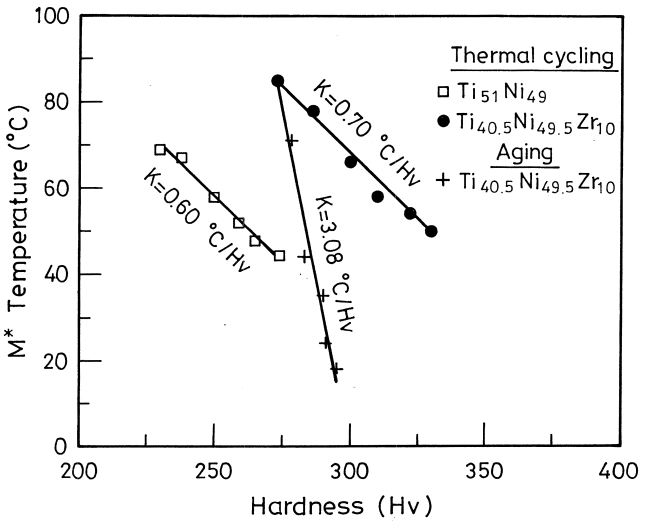

Fig. 10. The M* temperature versus hardness Hv for thermal cycled and aged $Ti_{40.5}Ni_{49.5}Zr_{10}$ alloy. The data for the thermal cycled $Ti_{51}Ni_{49}$ alloy are also included.

hardness to increase, as shown in Fig. 8 and Table 2. Therefore, both thermal cycling and aging can raise the yield stress $\Delta\sigma_y$. As derived from Eq. (1), this feature causes the M* (Ms) temperature to be lowered, as shown in Fig. 10. Upon carefully examining Fig. 10, it can be seen that the constant K of thermal-cycled $Ti_{40.5}Ni_{49.5}Zr_{10}$ alloy is slightly larger than that of thermal-cycled $Ti_{51}Ni_{49}$ alloy. We propose that the K value is related to the inherent hardness of annealed TiNi binary or TiNiX ternary alloys. The greater the annealed hardness is, the larger the K value will be. For example, the thermal-cycled $Ti_{40.5}Ni_{49.5}Zr_{10}$ alloy has its annealed hardness at 273 Hv and its K value at 0.70°C/Hv, which is larger than that of thermal-cycled $Ti_{51}Ni_{49}$ alloy (230 Hv, $K=0.60$°C/Hv). In other words, the depression of Ms (M*) temperature by the strengthening mechanism is stronger for the alloy having a higher annealed hardness.

The constant K of the thermal-cycled $Ti_{40.5}Ni_{49.5}Zr_{10}$ alloy ($K=0.70$°C/Hv) is smaller than that of the aged one ($K=3.08$°C/Hv). This feature is a result of different strengthening mechanisms, because the former strengthening originates from the thermal-cycled induced dislocations and the latter one results from the aging effects of point defects and atoms rearrangement in B2 phase. The fact that $K=3.08$°C/Hv $>>K=0.70$°C/Hv also indicates that the martensitic transformation temperatures of $Ti_{40.5}Ni_{49.5}Zr_{10}$ alloy can be more effectively depressed by aging in B2 phase than by B2↔B19′ thermal cycling.

4. Conclusion

1. The annealed $Ti_{40.5}Ni_{49.5}Zr_{10}$ alloy undergoes B2↔B19, one-stage martensitic transformation with Ms≈100°C. Many second phase particles $(Ti,Zr)_2Ni$ are found around the grain boundaries of (Ti,Zr)Ni matrix. Despite the existence of many second phase particles, this alloy still exhibits good shape recovery which can reach about 90%. The B19′ martensite structure is calculated as $a=0.295$ nm, $b=0.408$ nm, $c=0.491$ nm and $\beta=97.4^0$.
2. Transformation temperatures of $Ti_{40.5}Ni_{495}Zr_{10}$ alloy decrease and the hardness increases with increasing aging time at 300°C. This characteristic is related to the aging effects of point defects and atoms rearrangement in B2 phase. Besides, finer plates formed in $(001)_M$ compound twins for longer aged specimens may relate to these aging effects.
3. Transformation temperatures decrease and the hardness increases in the thermal-cycled $Ti_{40.5}Ni_{49.5}Zr_{10}$ alloy. The strengthening effect of thermal cycling and aging on transformation temperatures of this alloy is found to follow the equation $Ms=T_o-K\ \Delta\sigma_y$. Experimental results show that K values are associated with the alloy's annealed hardness. The Ti-rich $Ti_{40.5}Ni_{49.5}Zr_{10}$ alloy has solid-soluted Zr atoms and has a higher annealed hardness than the $Ti_{51}Ni_{49}$ alloy, and thus has a higher K value. Besides, the constant K of thermal-cycled $Ti_{40.5}Ni_{49.5}Zr_{10}$ alloy ($K=0.70$°C/Hv) is smaller than that of aged one ($K=3.08$°C/Hv). This result indicates that martensitic transformation temperatures of $Ti_{40.5}Ni_{49.5}Zr_{10}$ alloy can be more effectively depressed by aging in B2 phase than by B2↔B19′ thermal cycling.

Acknowledgements

The authors are grateful to Dr. T. S. Chou, Steel and Aluminum R and D Department, China Steel Corporation, for his great assistance with the internal friction measurement. The financial support of this study is provided by the National Science Council (NSC), Republic of China, under Grant No. NSC 86-2216-E002-033, is also sincerely appreciated.

References

[1] V.P. Sivokha, V.N. Khachin, Fizika Metallovi Metallovedenie 62 (1986) 534.
[2] V.N. Khachin, N.M. Matveea, V.P. Sivokha, Doklady AN SSSR 257 (1981) 167.
[3] S.K. Wu, C.M. Wayman, Metallography 20 (1987) 359.
[4] S.F. Hsieh, S.K. Wu, J. Alloys Comp. 266 (1998) 276.
[5] S.F. Hsieh, S.K. Wu, J. Alloys Comp. 270 (1998) 237.
[6] H.M. Rietveld, J. Appl. Crystallogr. 2 (1969) 65.
[7] J.H. Mulder, J.H. Mass, J. Beyer, ICOMAT, (1992) 869.
[8] H.C. Lin, S.K. Wu, J.C. Lin, Mater. Chem. Phys. 37 (1994) 184.
[9] S.H. Chen, Master's Thesis, Institute of Materials Science and Engineering, National Taiwan University, Taipei, Taiwan, 1994.
[10] H.C. Lin, S.K. Wu, Scripta Metall. 26 (1992) 59.

[11] C.M. Hwang, M. Meichle, M.B. Salamon, C.M. Waymam, Phil. Mag. A47 (1983) 9.
[12] X.D. Han, W.H. Zou, R. Wang, Z. Zhang, D.Z. Yang, K.H. Wu, J. De Physique IV (1995) C8–753.
[13] H.C. Lin, Ph.D. Thesis, Institute of Materials Science and Engineering, National Taiwan University, Taipei, Taiwan, 1992.
[14] J.S. Zhu, R. Schaller, W. Benoit, Phys. Lett. A141 (1989) 177.
[15] X.D. Han, W.H. Zou, S. Jin, Z. Zhang, D.Z. Yang, Scripta Metall. 32 (1995) 1441.
[16] D.T. Hawkins, R. Hultgren, ASM Handbook, Alloy Phase Diagram, Vol. 3, ASM International, Ohio, 1992, pp. 2-380.
[17] S. Miyazaki, T. Imai, Y. Igo, K. Otsuka, Metall. Trans. 17A (1986) 76.
[18] M. Cohen, E.S. Machlin, V.G. Paranjpe, Thermodynamics in Physical Metallurgy, ASM, Metals Park, OHIO, 1950.
[19] E. Hornbogen, Acta Metall. 33 (1991) 595.